Catalysis Communications 46 (2014) 51–56

Contents lists available at ScienceDirect

Catalysis Communications

journal homepage: www.elsevier.com/locate/catcom

Short Communication

Structural and catalytic properties of mesoporous nanocrystalline mixed oxides containing magnesium

N. Rezlescu [a,*], E. Rezlescu [a], L. Sachelarie [b], P.D. Popa [a], C. Doroftei [c]

[a] National Institute of Research and Development for Technical Physics, Iasi, Romania
[b] Apolonia University, Iasi, Romania
[c] Al.I. Cuza University, Physics Faculty, Iasi, Romania

ARTICLE INFO

Article history:
Received 7 June 2013
Received in revised form 30 October 2013
Accepted 21 November 2013
Available online 1 December 2013

Keywords:
Oxides
Sol–gel self-combustion growth
Electron microscopy (SEM), X-ray diffraction
Microstructure

ABSTRACT

Oxide compounds are promising catalysts for VOC flameless combustion. In this paper the catalyst properties of two Mg-containing oxide compounds with different crystalline structures and chemical compositions (Mg spinel ferrite and La–Pb–Mg–Mn–O perovskite) were investigated. The samples, prepared by a combined sol–gel and self-combustion method and heat treatment, were characterized using X-ray diffraction, scanning electron microscopy, EDAX spectroscopy, and BET analysis. The two samples have been catalytically tested in flameless combustion reaction of acetone, benzene and propane at atmospheric pressure. The results revealed a higher catalytic activity of the perovskite catalyst that may be ascribed to smaller crystallite size (26 nm), larger surface specific area (8.6 m^2/g) and the presence of manganese cations with variable valence (Mn^{3+}–Mn^{4+}).

1. Introduction

The use of perovskite or spinel type oxide compounds as catalysts for VOCs combustion has been widely investigated to find a catalyst with high thermal stability [1–4] and low temperature activity [5,6]. Mixed oxide systems are promising catalysts for catalytic combustion of volatile organic compounds (VOCs). The catalytic combustion is one of the most effective techniques for the removal of VOCs [7–9].

Many studies have focused on the lanthanum manganite perovskites $LaMnO_3$, which are known to be very good oxidation catalysts [10,11]. Lanthanum, the largest lanthanide ion, forms the most stable perovskite structure [12]. The partial substitution of La^{3+} ions in this stable structure by lower valence ions (such as Pb^{2+} and Mg^{2+} in the present work) can produce the partial oxidation of Mn^{3+} to Mn^{4+} ions and the increase in oxygen vacancies which enhance the catalytic activity of the perovskite [13,14]. Ponce et al. [15] found that the stability of Mn^{4+}ions seems to be the most important factor in the catalytic activity of perovskite type manganites. Previous investigations [16–18] showed a major role of manganese in the catalytic combustion of VOCs. The Mg substitution in $LaMnO_3$ should act as a structural promoter (inhibits the crystallite growth by reducing the grain boundary mobility [19]). Saracco et al. [20] reported on the positive effect of the Mg substitution in $LaMnO_3$ perovskite on the catalytic activity of the resulting perovskite. Rosso et al. [21] also showed the beneficial role of MgO which acts as a sulfur poisoning limiting agent in $LaMn_{1-x}Mg_xO_3$ perovskites, similar to the action observed with addition of noble metals, such as Pd or Pt. The effect of Pb addition in perovskites has been less investigated due to its toxicity. However, several research reports [22,23] have proven that the introduction of Pb^{2+} in the crystal lattice of the $LaMnO_3$ perovskite stimulates a high ratio of Mn^{4+}/Mn^{3+}, decreases the synthesis temperature, and improves the conductivity of the perovskite.

For catalytic purposes, the microstructure has a predominant role. The achievement of spinel ferrites or perovskites with the high specific surface areas and nanosized particles is a priority in the performance of a catalyst. In nanostructured materials, the interface between the nanoparticles and its surrounding medium plays a more important role than the bulk. Also, the strong curvature of nanoparticles due to their small radius leads to an increased number of the structural defects at the nanoparticle surface which enhance the surface reactivity. To obtain perovskites and spinel ferrites with superior microstructures, various chemistry based synthesis methods have been proposed, such as sol–gel [24], coprecipitation [25], hydrothermal [26], spray drying [27], combustion reaction [27], and other methods. Oliva et al. [28] found that the change in the preparation procedure can have a remarkable effect on the physico-chemical characteristics of perovskites. The catalytic activity is correlated with various physico-chemical properties [29].

In the present work we applied a nonconventional procedure, a combined sol–gel and self-combustion method [30] followed by thermal treatment. In this procedure the heat generated by an exothermic combustion reaction was used for synthesis reaction of the oxide ceramics. The intimate mixing of constituent ions so that nucleation and crystallization can occur at relatively low temperature is the main feature of this method. Sol–gel self-combustion method offers a number

* Corresponding author.
E-mail addresses: nicolae.rezlescu@gmail.com, reznic@phys-iasi.ro (N. Rezlescu).

1566-7367/$ – see front matter © 2013 Elsevier B.V. All rights reserved.
http://dx.doi.org/10.1016/j.catcom.2013.11.021

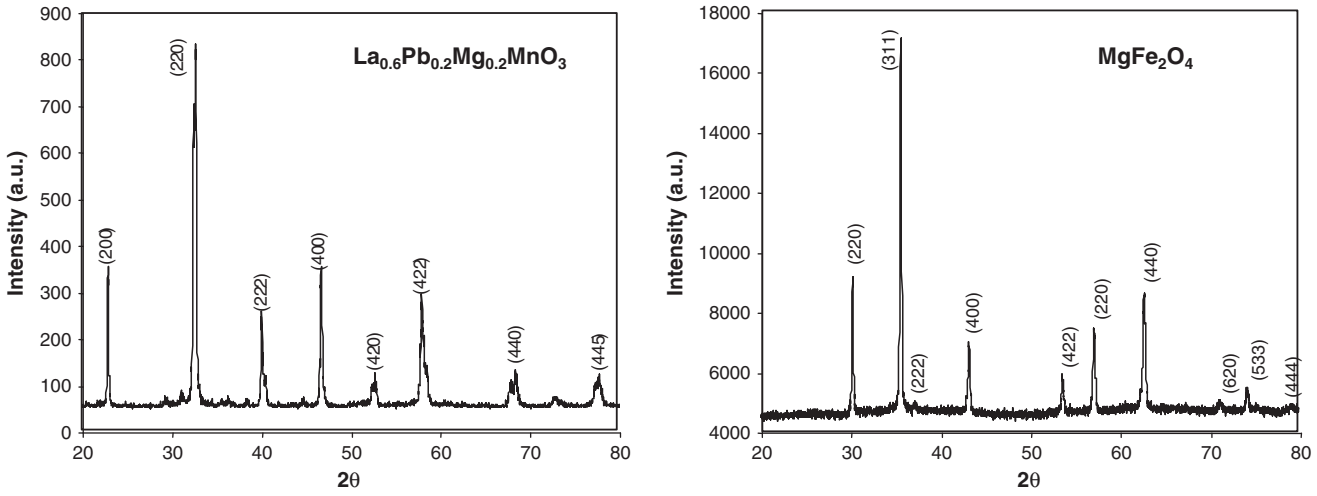

Fig. 1. XRD patterns for $La_{0.6}Pb_{0.2}Mg_{0.2}MnO_3$ and $MgFe_2O_4$ nanopowders.

of advantages including homogeneous mixing (on the atomic scale), high purity, low energy cost, simple equipment, easy manufacturing and the control of the grain size by subsequent heat treatments. By this procedure perovskites can be prepared at much lower temperature (1000 °C) in comparison with the temperature required for the conventional synthesis (1400–1600 °C). Using sol–gel coupled with combustion synthesis method and heat treatment at 950 °C, Tzimpilis et al. [31] prepared lanthanum based perovskites with enhanced catalytic activity in the methane flameless combustion. The main drawback of this method is that polluting compounds are emitted during the combustion (NH_3 or NO_x).

The purpose of this paper is to find new thermally and chemically stable solid state oxide compounds with suitable properties for VOCs combustion at low temperature. Spinel-type ferrite nanopowders of chemical composition $MgFe_2O_4$ and $La_{0.6}Pb_{0.2}Mg_{0.2}MnO_3$ perovskite nanopowders were investigated. We analyzed comparatively the catalyst properties of the two samples, which have different compositions and structures, in the catalytic flameless combustion of some VOCs: acetone, benzene and propane. The influence of various catalyst parameters (chemical composition, crystallite size, surface specific area) and of the process parameters (reaction temperature, conversion degree) on VOC catalytic combustion has been investigated.

2. Experimental

2.1. Sample preparation

$MgFe_2O_4$ spinel ferrite and $La_{0.6}Pb_{0.2}Mg0.2MnO_3$ perovskite have been prepared by sol–gel self-combustion method [30], using metal nitrates, ammonium hydroxide and polyvinyl alcohol (PVA) as starting materials. This method included the following steps:

(1) Dissolution of metal nitrates in deionized water.
(2) Polyvinyl alcohol (10% concentration) addition to nitrate solution to make a colloidal solution (metal/PVA ratio = 1).
(3) NH_4OH (10% concentration) addition to increase pH to about 8; a sol of metal hydroxides in polyvinyl alcohol and ammonium nitrate was obtained.
(4) Stirring at 80 °C for 10 min to turn the sol of metal hydroxides into viscous gel.
(5) Drying the gel at 100 °C for 12 h.
(6) *Self-combustion*. The dried gel was locally ignited by an electrically heated wire, triggering an exothermic reaction; once initiated, the combustion wave spontaneously auto propagated (less than 10 s) through the dried gel. During combustion reaction, the temperature is of about 1000 °C and the metal hydroxides convert into metal oxides and the nucleation of very fine crystallites takes place.
(7) Calcination at 500 °C for 30 min of the burnt powder to eliminate any residual organic compound (C, residual PVA).
(8) Heat treatment of the powders to improve the crystallinity of the materials. $MgFe_2O_4$ powder was treated at 900 °C for 20 min and $La_{0.6}Pb_{0.2}$ $Mg_{0.2}MnO_3$ was treated at 1000 °C for 120 min. The higher temperature for longer time interval for perovskite was preferred for two main reasons. First, the heat released by the combustion reaction is not sufficient to raise the system temperature to a level that allows the growth of the perovskite crystallites. Second, $La_{0.6}Pb_{0.2}$ $Mg_{0.2}MnO_3$ is an oxide compound and it is possible that the migration of ions required for the formation of the perovskite structure demands some residence time at high temperature. By heat treatment it was improved the crystallization of the perovskite phase and nanosized crystallites are obtained.

Table 1
Structure characteristics.

Sample composition	Lattice parameter (nm)	Crystal size (nm)	dx (g/cm^3)
$MgFe_2O_4$	0.8379	45.8	4.50
$La_{0.6}Pb_{0.2}Mg_{0.2}MnO_3$	0.7719	25.8	8.38

By this procedure oxide compounds with very fine crystallites can be prepared at a much lower temperature than the temperature required by the conventional ceramic method (1300–1500 °C).

2.2. Characterization techniques

Crystal structure and phase composition of the samples were analyzed by XRD. X-ray diffraction measurements of the powders were performed at room temperature using PANALYTICAL X' PERT PRO MPD powder diffractometer and CuKα radiation (λ = 1.542512 Å). The spectra were scanned between 20 and 80° (2θ) at a rate of 2°/min. The average crystallite size was evaluated based on XRD peak broadening using the Scherer equation $D = 0.9\lambda/\beta\cos\theta$, were λ is the radiation wavelength (0.15405 nm) of CuKα, β is the half width of the peak and θ is the Bragg diffraction peak angle. A scanning electron microscope (JEOL-200 CX) was used to observe the surface morphology. Textural characteristics were investigated by means of specific surface area determined by BET (Brunauer–Emmett–Teller) [32] method from the nitrogen sorption

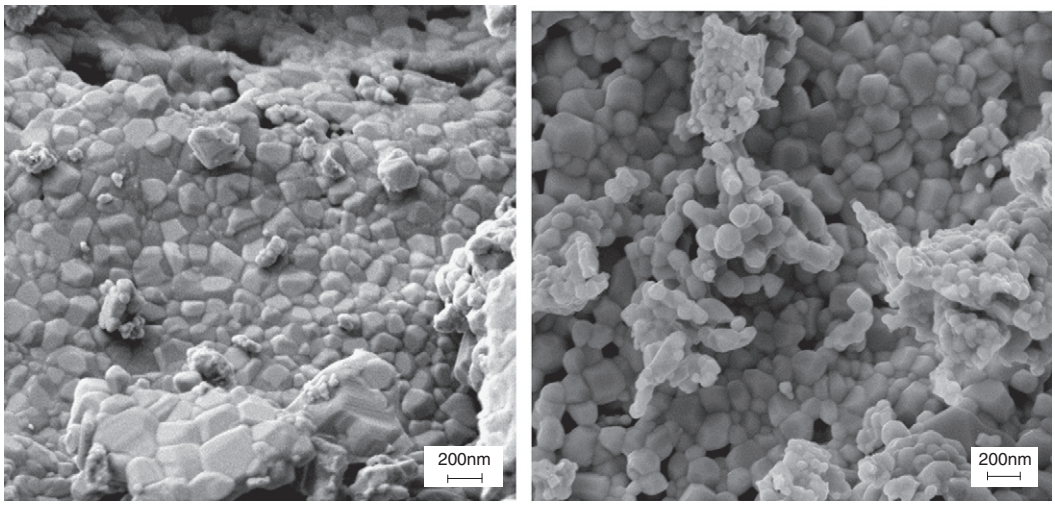

Fig. 2. SEM micrographs for $La_{0.6}Pb_{0.2}Mg_{0.2}MnO_3$ and $MgFe_2O_4$ nanopowders.

isotherms at 77 K. Adsorption/desorption isotherms were determined with NOVA-2200 apparatus. The pore size distribution (PSD) curves were obtained from sorption isotherms using BJH (Barret–Joyner–Halenda) method [32]. The chemical composition of the surface particles was examined with Energy Dispersive X-ray Spectrometer (EDS).

3. Results and discussion

3.1. Characterization of materials

The XRD patterns at room temperature of the heat treated samples are shown in Fig. 1. Results revealed that all samples were monophase

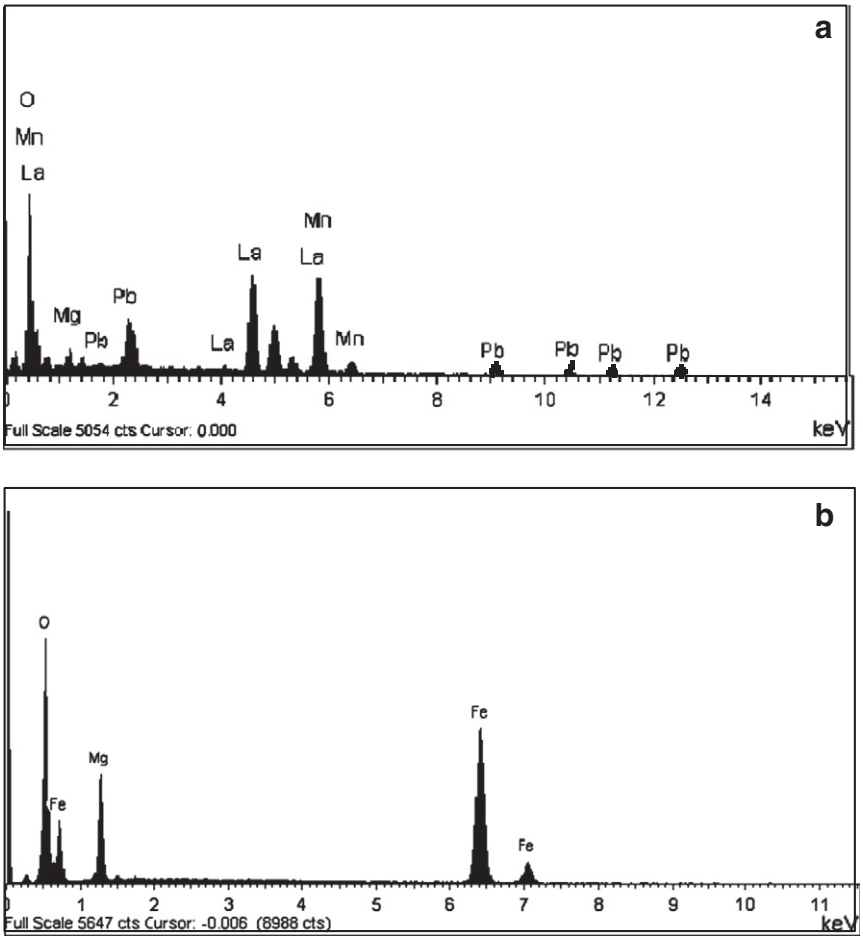

Fig. 3. EDAX spectrum for a) $La_{0.6}Pb_{0.2}Mg_{0.2}MnO_3$ perovskite heat treated at 1000 °C for 120 min and b) $MgFe_2O_4$ ferrite heat treated at 900 °C for 20 min.

Table 2
EDAX analysis of $La_{0.6}Pb_{0.2}Mg_{0.2}MnO_3$ and $MgFe_2O_4$ powders.

$La_{0.6}Pb_{0.2}Mg_{0.2}MnO_3$		$MgFe_2O_4$	
O (at %)	63.85	O (at %)	54.44
La (at %)	11.61	Mg (at %)	15.08
Mn (at %)	18.04	Fe (at %)	30.48
Mg (at %)	4.02	Mg/Fe	0.49
Pb (at %)	2.47		
(La + Mg + Pb)/Mn	1.01		

Table 3
Surface characteristics of $MgFe_2O_4$ and $La_{0.6}Pb_{0.2}Mg_{0.2}MnO_3$ powders.

Characteristics	$MgFe_2O_4$	$La_{0.6}Pb_{0.2}Mg_{0.2}MnO_3$
BET surface area (m^2/g)	3.9	8.6
BJH pore volume (cc/g)	0.006	0.0187
BJH average pore size (nm)	4.29	7.55
Particle size D_{BET}[a] (nm)	340.0	81.1

[a] D_{BET} was calculated using S_{BET} [32].

without any other second phase. Cubic spinel structure (Fd3m space group) was identified for $MgFe_2O_4$ sample and cubic perovskite structure (Fm3m space group) for $La_{0.6}Pb_{0.2}Mg_{0.2}MnO_3$. The lattice parameters and average crystallite size derived from XRD data are given in Table 1. The values of the lattice parameters almost coincide with those presented in the literature in analogous compounds [33,34]. It is evident that the nanosized crystallinity and that the crystallite size and density behave inversely to each other with respect to Mg concentration. Smaller crystal size (25.8 nm) and higher density (8.38 g/cm^3) were found in $La_{0.6}Pb_{0.2}Mg_{0.2}MnO_3$ perovskite which contains 20% molar Mg only.

SEM micrographs showing surface morphology of the two powders are shown in Fig. 2. One can note significant differences in the microstructure of the two samples. Small agglomerates of fine grains with irregular shape can be observed in the perovskite powder, whereas $MgFe_2O_4$ spinel powder is characterized by the presence of dense and larger agglomerates.

The EDAX patterns given in Fig. 3 confirm the purity of the chemical compositions. Table 2 summarizes the elemental compositions. The Mg/Fe and (La + Mg + Pb)/Mn ratio are found close to the theoretical value (0.5 and 1.0 respectively) and this is a proof of homogeneous distribution of the elements in the solid.

Nitrogen adsorption/desorption isotherms at ~77 K were used to obtain information about the specific surface area S_{BET}, the pore volume and the pore size in the ceramic particles. The isotherms for both samples are presented in Fig. 4. As can be seen, the desorption branch does not follow the adsorption branch, but forms a hysteresis loop of type H3 according to the International Union of Pure and Applied Chemistry (IUPAC) classification [32]. H3 type hysteresis is typical for materials with an interparticle mesoporosity (pore size 2–50 nm) [32]. However, a clear decision with regard to the type of hysteresis loop is not always possible. The factors which determine the shape of the hysteresis loop are still not fully known for disordered pore system.

Pore size distribution curves (PSD by BJH method) for both samples obtained from N_2 (~77 K) sorption isotherms are given in the insets in Fig. 4. The pore size distribution of $La_{0.6}Pb_{0.2}$ $Mg_{0.2}MnO_3$ is found to be different from that of $MgFe_2O_4$, but all pore sizes are within the mesoporous region (2–50 nm).

The BET surface area, pore volume and average pore diameter are given in Table 3. BET specific surface area (8.6 m^2/g) of $La_{0.6}Pb_{0.2}Mg_{0.2}$ MnO_3 is higher than that of $MgFe_2O_4$ (3.9 m^2/g). Larger pore volume and smaller particle size determine the increased S_{BET} value of the perovskite. The characteristics of MgFe2O4 ferrite and $La_{0.6}Pb_{0.2}Mg_{0.2}$ MnO_3 perovskite are comparable to those of other spinel ferrites and perovskites reported in [35–37].

3.2. Catalytic activity

The catalytic testing of the two catalyst samples in the flameless combustion of three VOCs (acetone, propane and benzene) was carried out at atmospheric pressure in a flow-type set-up previously described by us [38]. The catalyst powder (0.3–0.5 g) was sandwiched between two layers of quartz wool in a quartz tubular micro-reactor (ϕ = 7 mm) placed in an electrical furnace. The increase of the temperature was made stepwise. At every predetermined temperature, as a result of catalytic combustion, the gas concentration when exiting the reactor will be smaller than the inlet gas concentration. The degree of conversion of gasses over catalysts at a certain temperature was calculated as:

$$\text{Conv} = \frac{c_{in} - c_{out}}{c_{in}} \times 100\%,$$

where c_{in} and c_{out} are the inlet and outlet gas concentration, respectively, measured by a photo-ionization detector (PID-TECH) for VOCs. Data were collected when the flameless catalytic combustion had reached a steady state, after about 20 min at each temperature. These experiments were repeated decreasing the temperature and similar results were obtained.

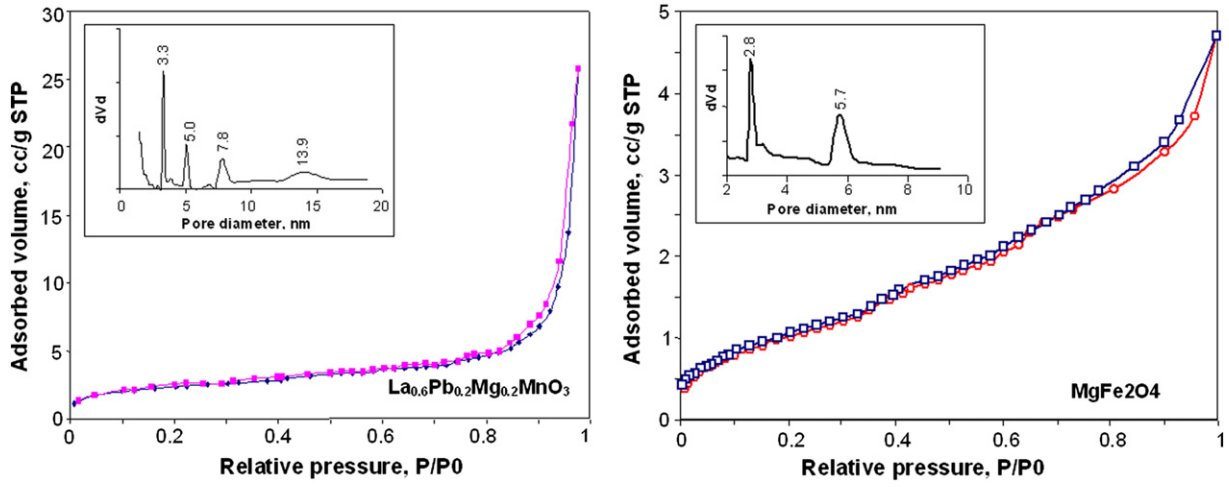

Fig. 4. N_2 adsorption/desorption isotherms at 77 K of the two powders: $La_{0.6}Pb_{0.2}Mg_{0.2}MnO_3$ perovskite and $MgFe_2O_4$ spinel ferrite (• o — the adsorption branch and ▪ □ — the desorption branch). Inset: the pore size distribution graphs.

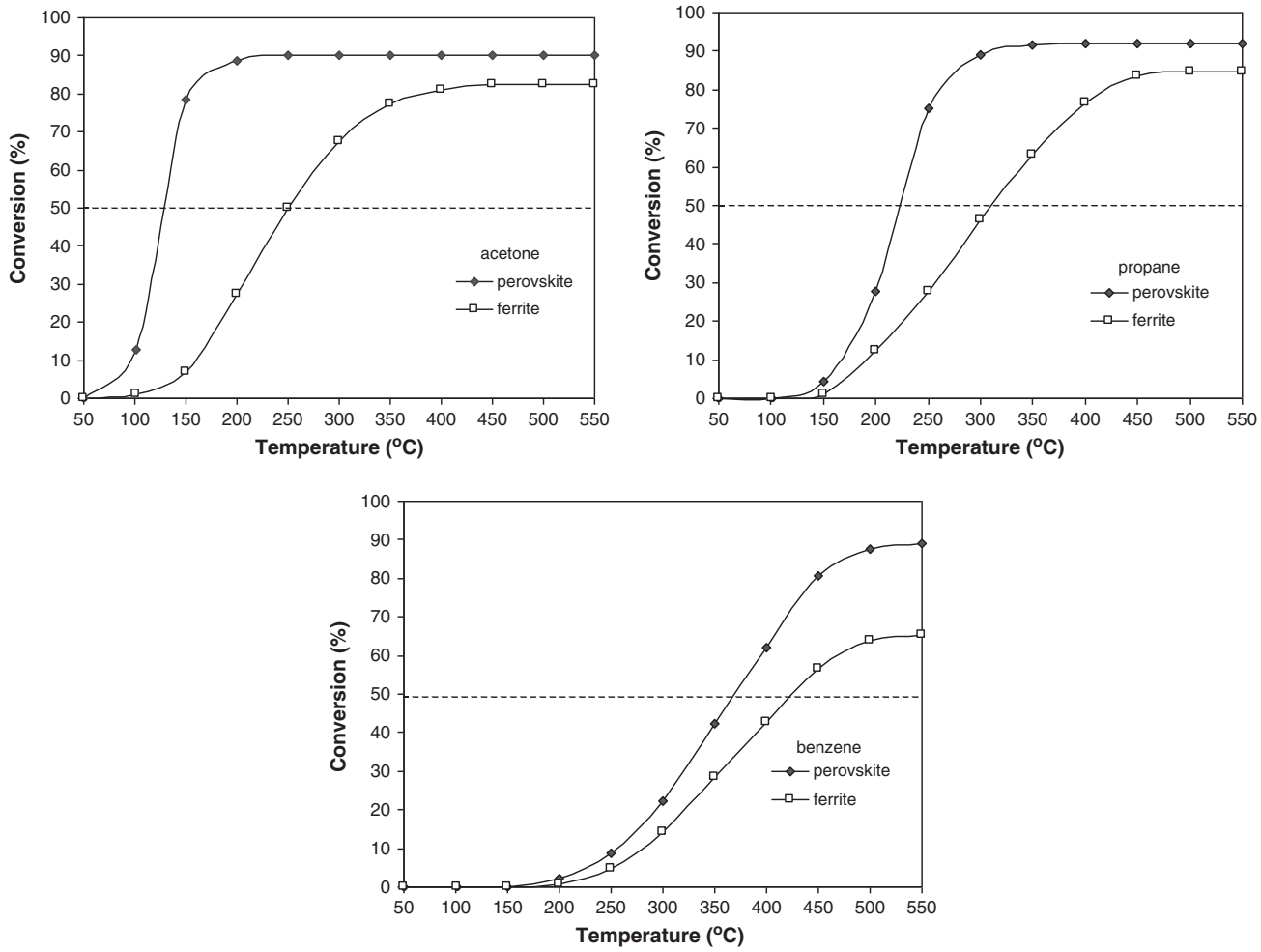

Fig. 5. Conversion of acetone, propane and benzene vs. temperature over $La_{0.6}Pb_{0.2}Mg_{0.2}MnO_3$ perovskite and $MgFe_2O_4$ spinel catalysts.

The catalytic reactions were investigated in the 20–550 °C range. Fig. 5 plots the VOC conversion over the two catalysts as a function of reaction temperature. One can note the followings: i) The catalytic activity of the two nanomaterials in the gas combustion is strongly influenced by the reaction temperature. Increasing the reaction temperature promotes gas conversion over the two catalysts. ii) The catalytic reactions involving ferrite catalyst occur at higher temperatures than in the presence of the perovskite catalyst. iii) The activities of the two catalysts differ significantly (Fig. 5). All experiments showed the $La_{0.6}Pb_{0.2}Mg_{0.2}MnO_3$ perovskite to be more active than the $MgFe_2O_4$ ferrite. The conversion degree of the gasses over perovskite catalyst may even exceed 90% at 500 °C, whereas over spinel catalyst the conversion is below 80%. The T_{50} values (T_{50} — the temperature necessary for a 50% gas conversion) can be used to appreciate the catalytic activity of the two catalysts: $MgFe_2O_4$ spinel and $La_{0.6}Pb_{0.2}Mg_{0.2}MnO_3$ perovskite. At T_{50} temperature the catalytic activity for the total oxidation of gasses is sufficiently high. The lower T_{50} is, the higher the activity is. In Fig. 5 it can be observed that the T_{50} values for acetone (128 °C) and propane (224 °C) conversion over the $La_{0.6}Pb_{0.}Mg_{0.2}MnO_3$ perovskite are lower (with about 100 °C) in comparison with those obtained with the $MgFe_2O_4$ catalyst (250 °C and 312 °C for acetone and propane respectively). The catalytic combustion data obtained by us are in agreement with those reported in the literature for similar systems [39,40].

The catalyst stability of the two materials was studied and no deactivation was observed in any of the samples after 24 h.

The better catalyst performance of $La_{0.6}Pb_{0.2}Mg_{0.2}MnO_3$ perovskite in comparison with $MgFe_2O_4$ spinel is likely to be attributed to the smaller crystallite size (26 nm), larger surface area (8.6 m^2/g) as well as the presence of manganese cations with variable valence. Redox titration method showed that $La_{0.6}Pb_{0.2}Mg_{0.2}MnO_3$ perovskite contains a considerable concentration of Mn^{4+} ions (35%) in addition to Mn^{3+} ions, which form to compensate the charge change caused by Mg^{2+} and Pb^{2+} substitutions for La^{3+}. The presence of Mn^{3+}–Mn^{4+} ions implies oxygen vacancies which favor the increase in the oxygen ion species (O^-, O_2^-, O^{2-}) adsorbed on perovskite surface [41]. Although the mechanism behind the catalytic activity of the perovskites is still debated, the interaction of surface active oxygen species with reactants (suprafacial mechanism) is widely accepted to explain the complete hydrocarbons oxidation over mixed oxide catalysts [37,42]. According to accepted opinion, at low temperatures (below 400 °C) the catalytic activity of the oxides in the total oxidation reactions of the gasses is determined by the amount of weakly bound surface oxygen species [37]. The weaker the oxygen binding at the catalyst surface is, the more active is the catalyst for complete oxidation of gasses. The surface oxygen species (O^-, O_2^-, O^{2-}) involved in the catalytic oxidation may come from the gaseous molecular oxygen or from the lattice oxygen. We have not excluded the involvement of the lattice oxygen although its mobility is smaller than that of surface adsorbed oxygen. The formation of the defective structures in the perovskite structure by partial substitution of La^{3+} by ions of lower valence (Mg^{2+}, Pb^{2+}) will facilitate the mobility of the lattice oxygen (via oxygen vacancy mechanism [43]) and the material will be more active for oxidation reactions [44].

In the present study, the difference in the catalytic activity of the two catalysts in the combustion of acetone, propane and benzene may result

from the different reactivities or amounts of the active oxygen species involved in the combustion reaction, or from a variation in the number of active sites on the catalyst surface determined by the specific structural properties of each material. Of course, the roles of the specific surface area and particle size are very important. A larger surface area will imply many more interactions between the perovskite surface and the test gasses and therefore high catalytic activity towards VOC combustion. The obtained results allow one to conclude that the $La_{0.6}Pb_{0.2}Mg_{0.2}MnO_3$ perovskite may be a promising catalyst for catalytic flameless combustion of acetone and propane at low temperatures (below 300 °C).

4. Conclusions

In this work the combined sol–gel and self-combustion method has been employed to prepare $MgFe_2O_4$ spinel and $La_{0.6}Pb_{0.2}Mg_{0.2}MnO_3$ perovskite for catalyst applications. It is an inexpensive method and the obtained products were pure and presented nanosized crystallinity. Both samples have been tested in the catalytic combustion of acetone, propane and benzene. $La_{0.6}Pb_{0.2}Mg_{0.2}MnO_3$ catalyst is more active at low temperatures compared to $MgFe_2O_4$ catalyst. The observed higher catalytic activity with the perovskite catalyst (over 90% gas conversion) is likely to be attributed to the smaller crystallite size (26 nm), higher specific area (8.6 m^2/g), and the presence of manganese cations with variable valence (Mn^{3+}–Mn^{4+}).

$La_{0.6}Pb_{0.2}Mg_{0.2}MnO_3$ perovskite may be a promising catalyst for catalytic combustion of acetone and propane at low temperatures (bellow 300 °C).

Acknowledgments

This work was supported by a grant of the Romanian National Authority for Scientific Research, CNST–UEFISCDI, project number PN-II-ID-PCE-2011-3-0453.

References

[1] T. Seiyama, in: L.G. Tejuka, G.L.G. Fierro (Eds.), Preparation and Application of Perovskite-type Oxides, Marcel Decker, 1993, p. 215.
[2] S. Cimino, L. Lisi, R. Pirone, G. Russo, M. Turco, Catal. Today 59 (2000) 19–31.
[3] E. Campagnoli, A. Tavares, L. Fabbrini, I. Rossetti, Y.A. Dubitsky, A. Zaopo, L. Forni, Appl. Catal. B Environ. 55 (2005) 133–139.
[4] A.C.F.M. Costa, R.T. Lula, R.H.G.A. Kiminami, L.F.V. Gama, A.A. de Jesus, H.M.C. Andrade, J. Mater. Sci. 41 (2006) 4871–4875.
[5] L.D. Pfefferle, W.C. Pfefferle, Catal. Rev. Sci. Eng. 29 (1987) 219–267.
[6] H. Arai, H. Fukuzawa, Catal. Today 26 (1995) 217–221.
[7] W.B. Li, J.X. Wang, H. Gong, Catal. Today 148 (2009) 81–87.
[8] A.V. Murugan, V. Samuel, S.C. Navale, V. Ravi, Mater. Lett. 60 (2006) 17911792.
[9] M. Epifani, E. Melissano, G. Pace, M. Schiopa, J. Eur. Ceram. Soc. 27 (2007) 115–123.
[10] N. Yamazoe, Y. Teraoka, Catal. Today 8 (1990) 170.
[11] H.M. Zhang, Y. Shimizu, Y. Teraoka, N. Mium, N. Yamazoe, J. Catal. 121 (1990) 432–440.
[12] M.A. Pena, J.L.G. Fierro, Chem. Rev. 107 (2001) 1931–2017.
[13] A. Kaddouri, P. Gelin, N. Dupont, Catal. Commun. 10 (2009) 1085–1089.
[14] R.M.G. de la Cruz, H. Falcon, M.A. Pena, J.I.G. Fierro, Appl. Catal. B Environ. 33 (2001) 45–55.
[15] S. Ponce, M.A. Pena, J.L.G. Fierro, Appl. Catal. B Environ. 24 (2000) 193–205.
[16] S.K. Samantaray, K.M. Parida, Appl. Catal. B Environ. 57 (2005) 83–91.
[17] T. Mishra, P. Mohapatra, K.M. Par, Appl. Catal. B Environ. 79 (2008) 279–285.
[18] K.M. Parida, Amarendra Samal, Appl. Catal. A Gen. 182 (1999) 249–256.
[19] J. Zao, M.P. Harmer, J. Am. Ceram. Soc. 70 (1987) 860–866.
[20] G. Saracco, F. Geobaldo, G. Baldi, Appl. Catal. B Environ. 20 (1999) 277–288.
[21] I. Rosso, G. Saracco, V. Speccia, E. Garrone, Appl. Catal. B Environ. 40 (2003) 195–205.
[22] N. Chau, H.N. Nhat, N.H. Luong, D.L. Minh, N.D. Tho, N.N. Chau, Physica B 327 (2003) 270–278.
[23] A. Staneva, Y. Dimitriev, Y. Ivanova, E. Kashchieva, J.M. Viera, M. Kolev, J. Univ.Chem. Tech. Met. 42 (2007) 55–60.
[24] N. Chu, X. Wang, Y. Liu, H. Jin, Q. Wu, L. Li, Z. Wang, H. Ge, J. Alloys Comp. 470 (2009) 438–442.
[25] A.B. Gadkari, T.J. Shinde, P.N. Vasambekar, Mater. Chem. Phys. 114 (2009) 505–510.
[26] X. Li, G. Wang, J. Magn. Magn. Mater. 321 (1276) (2009).
[27] A.C.F.M. Costa, R.T. Lula, R.H.G.A. Kiminami, L.F.V. Gama, A.A. de Jesus, H.M.C. Andrade, J. Mater. Sci. 41 (2006) 4871.
[28] C. Oliva, L. Bonoldi, S. Cappelli, L. Fabbrini, I. Rossetti, L. Forni, J. Mol. Catal. A Chem. 226 (2005) 33–40.
[29] N.N. Das, K.M. Parida, B.C. Tripathy, S.B. Rao, Ind. J. Chem. Sect. A 33 (1994) 820–825.
[30] P.D. Popa, N. Rezlescu, G.h. Iacob, A new procedure for preparing ferrite powders, Romanian Patent No.121300, OSIM, Bucharest, 2008.
[31] E. Tzimpilis, N. Moschoudis, M. Stoukides, P. Bekiaroglou, Appl. Catal. B Environ. 84 (2008) 607–615.
[32] S. Lowell, J.E. Shields, M.A. Thomas, M. Thommes, Characterization of Porous Solids and Powders: Surface Area, Pore Size and Density, Kluwer Academic Publishers, Dordrecht/Boston/London, 2004.
[33] R. Mahendiran, R. Mahesh, A.K. Raychaudhuri, C.N.R. Rao, J. Phys. D. Appl. Phys. 28 (1995) 1743–1745.
[34] N.G. Pirogova, N.M. Panich, R.I. Korosteleva, Yu.V. Voronin, G.E. Kalinina, Russ. Chem. Bull. 45 (1996) 42–44.
[35] N. Rezlescu, E. Rezlescu, P.D. Popa, E. Popovici, C. Doroftei, M. Ignat, Mater. Chem. Phys. 137 (2013) 922–927.
[36] N. Rezlescu, C. Doroftei, E. Rezlescu, P.D. Popa, L. Sachelarie, J. Optoelectron. Adv. Mater. 15 (2013) 62–65.
[37] N. Rezlescu, E. Rezlescu, P.D. Popa, C. Doroftei, M. Ignat, J. Mater. Sci. 48 (2013) 4297–4304.
[38] R. Spinicci, M. Faticanti, P. Marini, S. De Rossi, P. Porta, J. Mol. Catal. A Chem. 197 (2003) 147–153.
[39] P.R.N. Silva, A.B. Soares, Ecletica Quim. 34 (2009) 31–38.
[40] J. Shu, S. Kaliaguine, Appl. Catal. B Environ. 16 (1998) L303–L308.
[41] D. Hirabayashi, T. Yosikawa, Y. Kawamoto, K. Mockizuki, K. Suzuki, Adv. Sci. Technol. 45 (2006) 2169–2175.
[42] D.V. Ivanov, L.G. Pinaeva, E.M. Sadovskaya, L.A. Isupova, Kinet. Catal. 52 (2011) 401–408.
[43] A.A. Taskin, A.N. Lavrov, Yoichi Ando, Prog. Solid State Chem. 35 (2007) 481–490.
[44] D.V. Ivanov, E.M. Sadovskaya, L.G. Pinaeva, L.A. Isupova, J. Catal. 267 (2009) 5–13.